Hindawi
International Journal of Optics
Volume 2023, Article ID 4053258, 7 pages
https://doi.org/10.1155/2023/4053258

Research Article

Design and Analysis of Target Simulator Using All Spherical System with High Matching Rate

Shijie Li [1,2] Xiaojing Zhang,[2] Kai Zhao,[2] Zihuai Li,[3] Xiong Li,[3] Lumin Zhao,[2] Jin Zhang,[1] and Changlong Cai[1]

[1]*Shaanxi Province Key Laboratory of Thin Film Technology and Optical Test, Xi'an Technological University, Xi'an, Shaanxi 710021, China*
[2]*Opto Electronic Group Henan Pingyuan Optics Electronics Co. Ltd, Jiaozuo 454000, China*
[3]*Wuhan Red Star Yang Science and Technology Co. Ltd, Wuhan 430014, China*

Correspondence should be addressed to Shijie Li; lishijie@xatu.edu.cn

Received 14 March 2023; Revised 5 May 2023; Accepted 22 August 2023; Published 8 September 2023

Academic Editor: Sulaiman W. Harun

To achieve low wavefront error and high throughput with vignetting-free target simulators, a concave-convex-concaveoff-axis spherical system is designed in this paper, which effectively eliminates astigmatism and coma of the system by fields of view (FOVs) and aperture offset and provides theoretical basis for the realization of 100% matching between the exit pupil of the field lens and entrance pupil of the three-mirror anastigmat (TMA) system. Only spherical mirror element is used in this target simulator, which not only reduces the difficulty of manufacturing and cost but also greatly reduces the difficulty of assembling and adjusting. It provides an effective scheme for the design of target simulator and has strong engineering application value.

1. Introduction

With the rapid development of remote sensing, optical systems are moving toward a large FOV and high resolution in many fields, such as space exploration, earth science, and military applications [1–3]. These optical systems are generally characterized by large aperture, high precision, and long focal length. In the detection process of the optical system, it is necessary to use small-diameter equivalent target to detect and monitor the manufacturing accuracy of the system; so, the target simulator was born. Sullivan et al. described the capabilities, design, manufacturing and integration status, and uses of OSIM, an optical simulator of the James Webb Space Telescope (JWST) Optical Telescope Element (OTE) [4]. Toshihiro proposed a design approach of a coaxis double TMA for designing a target simulator with a large field of view (FOV) [5]. TMA optical systems have strong aberration correction ability, so that it is easy to get larger FOV, larger relative aperture, and better imaging quality [6, 7]. Taking the famous Large Synoptic Survey Telescope (LSST) as an example, this coaxial TMA telescope with a FOV of 3.5° is composed of an 8.4 m primary mirror, a 3.4 m second mirror, and a 5.0 m tertiary mirror [8]. Off-axis TMA systems have great potential to provide good optical solutions to meet the requirement of high resolution while maintaining a large FOV [9–12]. Off-axis configurations usually make the aperture stop offset or the FOV biased to avoid obscuration and achieve a large FOV [13, 14].

In order to reduce the difficulty of manufacturing, cost, and installation of target simulator, a target simulator is proposed and designed, which is consisted only with spherical mirror. Also, the rotationally asymmetric aberrations which are mainly astigmatism and coma are eliminated based on FOVs and aperture offset. The engineering feasibility of the design of the target simulator has been confirmed by simulation analysis.

2. Selection of the Initial Configuration

For off-axis TMA systems with relay images, there are two types of configuration design that are widely adopted: concave-convex-concave systems and convex-concave-convex systems [7, 15].

The initial structure of the target simulator is from Offner spectrometer structure. Offner spectrometer consisted by three mirrors, and it is a finite remote imaging system. Concave-convex-concave systems have a strong ability to correct spherical, coma, astigmatism, and field curvature aberrations. In this paper, the finite remote target simulator is realized by matching the exit pupil of the field lens with the entrance pupil of the convex-concave-convex TMA system, and the optical path is shown in Figure 1(a). To simulate the finite optical path of the imaging system, the image plane and exit pupil of the imaging system are taken as the object plane and entrance pupil of the target simulator, respectively, as shown in Figure 1(b). The exit pupil of the TMA system is located behind the primary mirror (PM), and all mirrors are spherical, which reduces the difficulty of processing and assembling of the system. The marginal ray tracing of the system is shown in Figure 2.

To match the optical path of the imaging system, we focus on tracing the marginal ray behind the primary image plane, and the propagation of the marginal ray is illustrated in Figure 3. u is the paraxial ray's incident aperture angle with respect to the optical axis, u' is the corresponding exit aperture angle, y represents the heights of the marginal ray, and t_1, t_2, t_3, and t_4 represent the distance between the entrance pupil and PM, the distance between PM and the secondary mirror (SM), the distance between SM and the tertiary mirror (TM), and the distance between TM and the image plane, respectively.

We set transmission media refractive index as $n_1 = n_2' = n_3 = 1$, $n_1' = n_2 = n_3' = -1$. For PM, the optical power can be determined as

$$\varphi_i = (n_i' - n_i)c_i = \frac{2}{r_i}, \tag{1}$$

where i ($i = 1, 2, 3, 4$) represents the PM, SM, TM, and the image plane, respectively, and c_i and r_i is the curvature and radius.

By the paraxial ray tracing, the relationship between the ray height and the ray slope on different mirrors can be expressed as follows [16]:

$$\begin{cases} n_i'u_i' = n_i u_i - y_i\varphi_i, \\ y_{i+1} = y_i + u_i't_i', \\ t_i' = t_{i+1}, \\ u_i' = u_{i+1}. \end{cases} \tag{2}$$

Similarly, the ray tracing of the chief ray can be expressed as follows:

$$\begin{cases} n_i'\overline{u}_i' = n_i \overline{u}_i - \overline{y}_i\varphi_i, \\ \overline{y}_{i+1} = \overline{y}_i + \overline{u}_i't_i', \\ \overline{t}_i' = \overline{t}_{i+1}, \\ \overline{u}_i' = \overline{u}_{i+1}. \end{cases} \tag{3}$$

According to the Seidel aberration theory, in a rotationally symmetric optical system, five monochromatic aberrations, including spherical aberration (S_{I}), coma (S_{II}), astigmatism (S_{III}), field curvature (S_{IV}), and distortion (S_{V}), can be simplified as follows:

$$\begin{cases} S_{\mathrm{I}} = -\sum A^2 \cdot y \cdot \Delta\left(\dfrac{u}{n}\right), \\ S_{\mathrm{II}} = -\sum \overline{A}A \cdot y \cdot \Delta\left(\dfrac{u}{n}\right), \\ S_{\mathrm{III}} = -\sum \overline{A}^2 \cdot y \cdot \Delta\left(\dfrac{u}{n}\right), \\ S_{IV} = -\sum H^2 \cdot c \cdot \Delta\left(\dfrac{1}{n}\right), \\ S_V = -\sum \left\{ \dfrac{\overline{A}^3}{A} \cdot y \cdot \Delta\left(\dfrac{u}{n}\right) + \dfrac{\overline{A}}{A} \cdot H^2 \cdot c \cdot \Delta\left(\dfrac{1}{n}\right) \right\}, \end{cases} \tag{4}$$

where A and $\overline{A}$ represent the Snell invariant of the marginal ray and chief ray, respectively, and H is the Lagrange invariant, which can be calculated as follows:

$$\begin{cases} A = n(yc + u), \\ \overline{A} = n(\overline{y}c + \overline{u}), \\ \Delta\left(\dfrac{u}{n}\right) = \dfrac{u'}{n'} - \dfrac{u}{n}, \\ \Delta\left(\dfrac{1}{n}\right) = \dfrac{1}{n'} - \dfrac{1}{n}, \\ H = n\overline{u}y - nu\overline{y}. \end{cases} \tag{5}$$

In this paper, our main concerns are about the coma and astigmatism of the TMA. For a general optical design process, a specific Seidel coefficient is expected to be zero to meet different design requirements. An initial configuration is obtained by setting reasonable initial values.

3. Off-Axis TMA Systems Design

The parameters of the system are shown in Table 1. The FOV distribution of the object space is shown in Figure 4, and ray tracing in different FOVs is marked with different colors. The PM, SM, and TM are tilted and eccentric to obtain the initial configuration of the TMA system without central

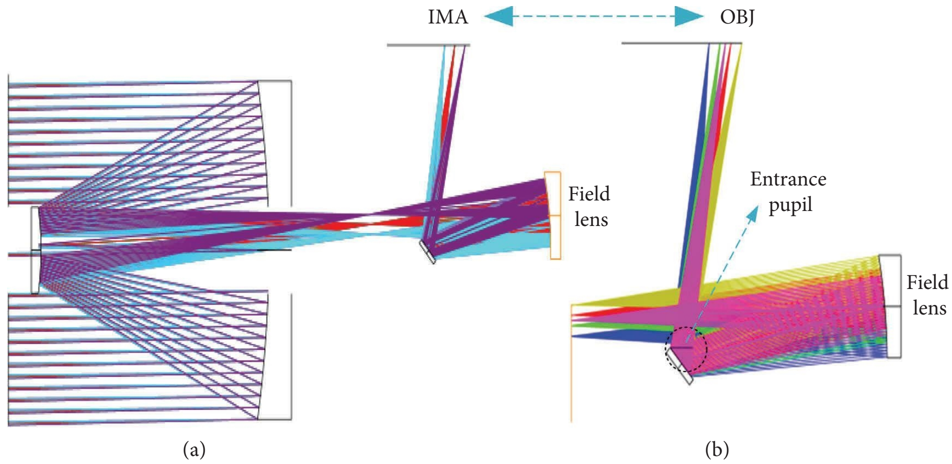

Figure 1: Imaging optical path.

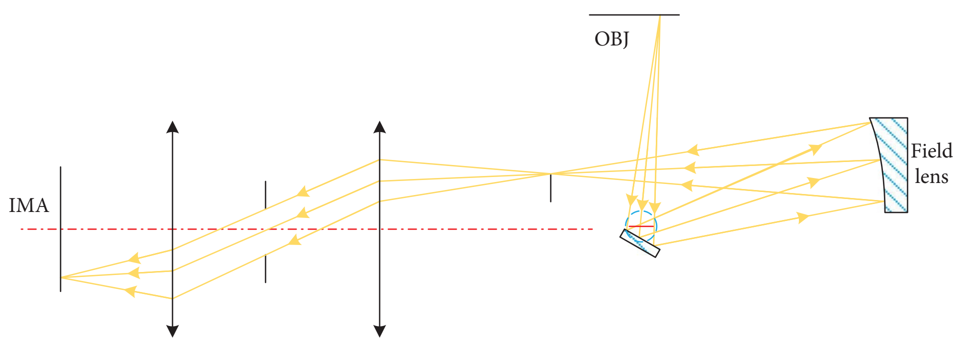

Figure 2: Principle diagram of the marginal ray tracing.

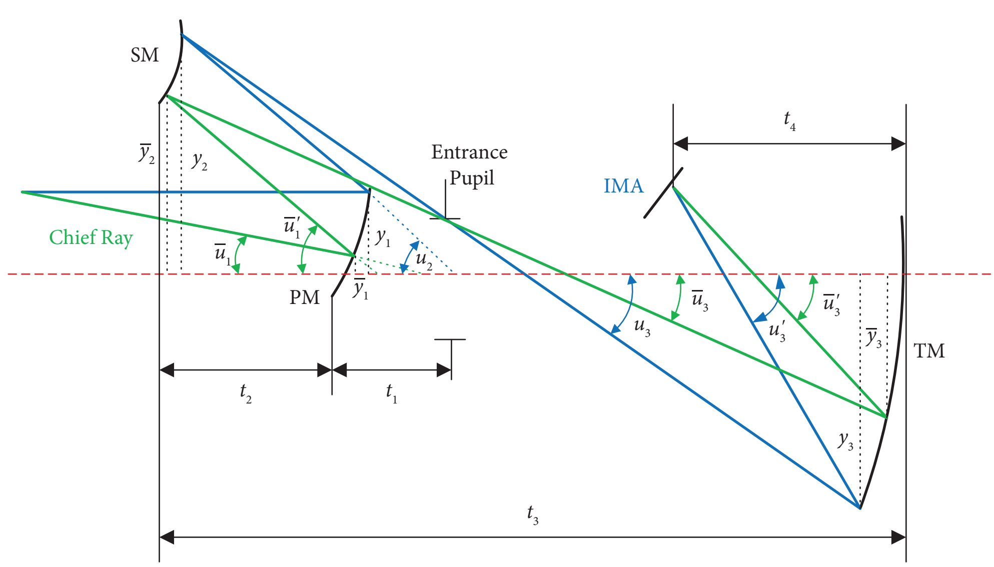

Figure 3: Ray tracing of the initial coaxial TMA configuration.

Table 1: Design parameters.

Parameters	Value
F number	10
Entrance pupil diameter	40 mm
Spectral range	0.43~0.8 μm
Magnification	1 : 1
Detector pixel size	16 μm

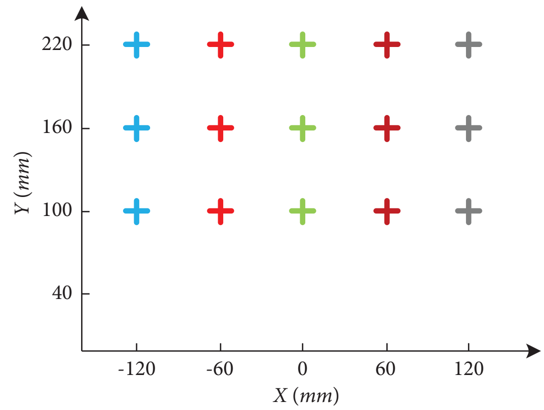

Figure 4: FOV distribution of the object space.

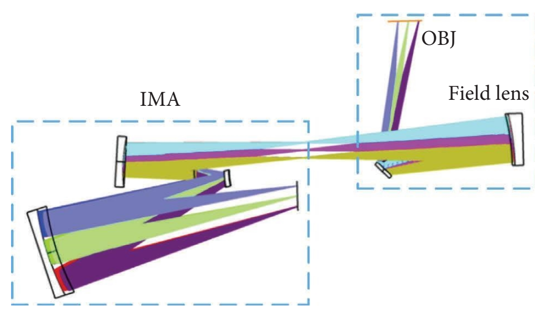

Figure 5: Initial configuration of the off-axis TMA system.

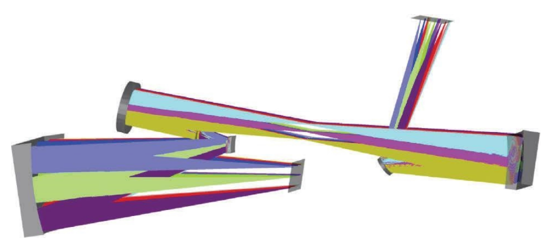

Figure 6: Optical layout of the final target simulator.

Table 2: Parameters of final configuration.

Surfaces	Radius	Distance (mm)	Decenter Y (mm)	Tilt X (°)
OBJ	Infinity	800.9	0	0
STO	Infinity	767.5	0	0
Fold mirror	Infinity	−750	0	45
Field lens	1389.2 mm	2250	0	0
PM	−979.63 mm	−586	−80	4.66
SM	−427.76 mm	1032.5	98.6	−13.17
TM	−1559.07 mm	−1434.08	443.3	−16.69

Figure 7: Spot diagram of the final target simulator.

obscuration, as shown in Figure 5. The off-axis system is an effective way to avoid the system blocking and vignetting. Therefore, these two phenomena need not be considered in the following analysis.

4. Design Results and Tolerance Analysis

4.1. Design Results. The structure of the final optical system is very compact, as shown in Figure 6. The detailed parameters of the system are listed in Table 2. It can be seen in Figure 7 that the spot radius in the spectral range of 0.43~0.8 μm is within a single pixel. Figure 8 shows the modulation transfer function (MTF) of the system and the MTF is greater than 0.5 at 34 lp/mm.

4.2. Tolerance Analysis. The tightness of the tolerance directly determines the difficulty of the processing and assembly of the system, so it is necessary to reasonably allocate the tolerance of the system, and the tolerance distribution is listed in Table 3.

We performed 100 simulations using Monte Carlo analysis to predict the performance. The diffractions MTF of the system in different FOVs under different probability distributions are listed in Table 4.

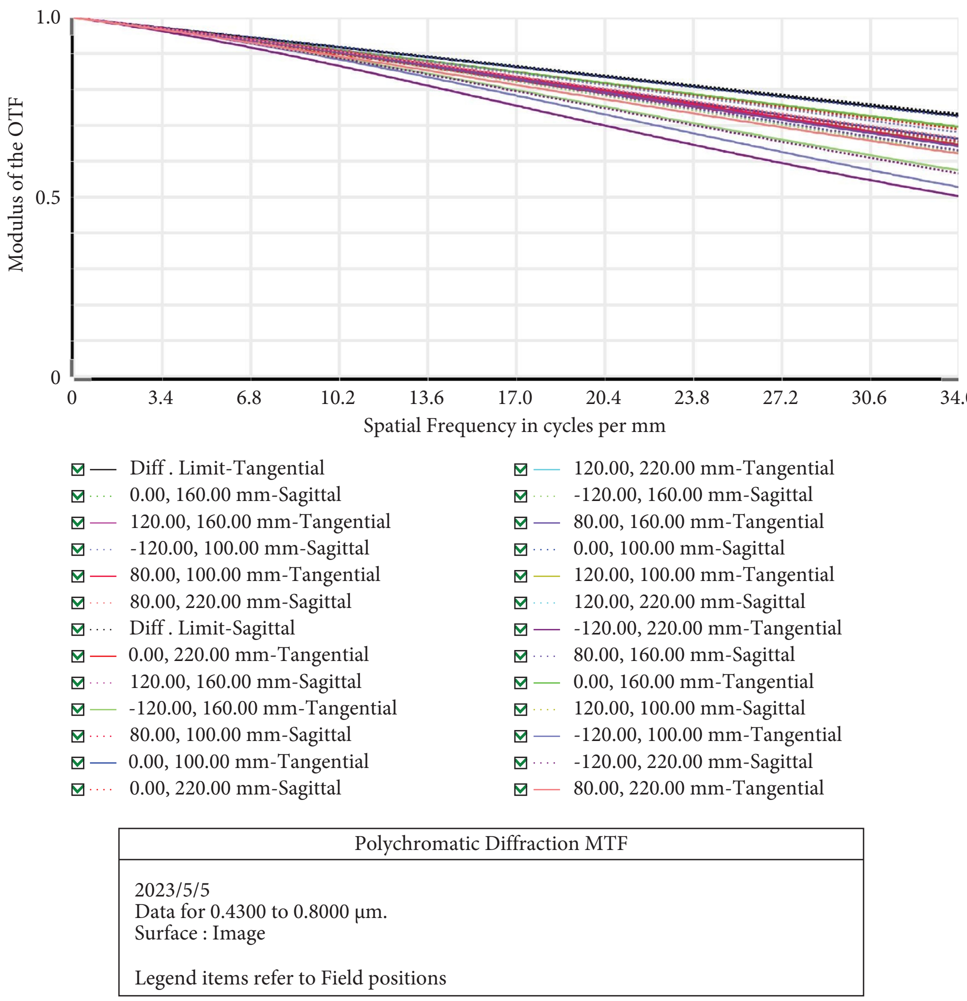

FIGURE 8: MTF of the final target simulator.

TABLE 3: Tolerance settings.

Surfaces	Δx (mm)	Δy (mm)	Δz (mm)	$\Delta\theta x$	$\Delta\theta y$	RMS/λ
Fold mirror	—	—	0.1	30″	30″	1/20
Field lens	—	—	—	—	—	1/30
PM	0.05	0.05	0.05	40″	40″	1/30
SM	0.08	0.08	0.08	35″	35″	1/30
TM	0.05	0.05	0.05	40″	40″	1/30

TABLE 4: Monte Carlo tolerance analysis probability results of MTF.

Probability (%)	Average MTF	MTF of center area	MTF of 0.707 area	MTF of marginal area
10	0.632	0.675	0.625	0.616
50	0.620	0.621	0.602	0.558
90	0.608	0.615	0.565	0.534

5. Conclusion

In this paper, by ray tracing of the concave-convex-concave coaxial system, the initial configuration in which the exit pupil of the TMA system is matched with the entrance pupil of the field lens is obtained, and the astigmatism and coma of the system are eliminated based on FOVs and aperture offset. By optimizing the eccentricity and tilt of the PM, SM, and TM, a low wavefront error and high throughput with vignetting-free target simulator is designed. Finally, we analyze the tolerance and engineering feasibility of the system, which confirms the validity of the target simulator that all mirrors are spherical.

Data Availability

The simulation analysis data used to support the findings of this study are included within the article.

Conflicts of Interest

The authors declare that they have no conflicts of interest.

Acknowledgments

The research was funded by Project of Shaanxi Provincial Science and the Technology Department (Grant no. 2022GY-222) and "Belt and Road" Innovative Talent Exchange Program for Foreign Experts (Grant no. DL2022040006L).

References

[1] M. B. Rakich and G. Pentland, "The Sky Mapper wide field telescope," *Proceedings of SPIE- The International Society for Optical Engineering*, vol. 6267, p. 62670E, 2006.

[2] M. Bolden and P. Kervin, "Panoramic-survey telescope and rapid response system: leveraging astronomical technology for satellite situational awareness," *38th COSPAR Scientific Assembly*, vol. 38, p. 3, 2010.

[3] P. Schipani, M. Capaccioli, and C. Arcidiacono, "VST: from commissioning to science," *Proceedings of SPIE- The International Society for Optical Engineering*, vol. 8444, p. 84441C, 2012.

[4] J. Sullivan, B. Eichhorn, and R. V. Handorf, "Manufacturing and integration status of the JWST OSIM optical simulator," *Proceedings of SPIE- The International Society for Optical Engineering*, vol. 7731, p. 77313V, 2010.

[5] T. Tsuzuki, "Optical design approach "co-axis double three-mirror anastigmat" for vignetting-free off-axis reflective relay optics," *Applied Optics*, vol. 58, no. 12, pp. 3247–3251, 2019.

[6] X. Liu, T. Gong, G. Jin, and J. Zhu, "Design method for assembly-insensitive freeform reflective optical systems," *Optics Express*, vol. 26, no. 21, pp. 27798–27811, 2018.

[7] Q. Meng, H. Wang, and K. Wang, "Off-axis three-mirror freeform telescope with a large linear field of view based on an integration mirror," *Applied Optics*, vol. 55, no. 32, pp. 8962–8970, 2016.

[8] J. Sebag, W. Gressler, and T. Schmid, "LSST telescope alignment plan based on nodal aberration theory," *Publications of the Astronomical Society of the Pacific*, vol. 124, no. 914, pp. 380–390, 2012.

[9] J. Zhu, W. Hou, X. Zhang, and G. Jin, "Design of a low F-number freeform off-axis three-mirror system with rectangular field-of-view," *Journal of Optics*, vol. 17, no. 1, Article ID 015605, 2014.

[10] Q. Meng, H. Wang, and W. Liang, "Design of off-axis three-mirror systems with ultrawide field of view based on an expansion process of surface freeform and field of view," *Applied Optics*, vol. 58, no. 3, pp. 609–615, 2019.

[11] Y. J. Ju, J. H. Jo, and J. M. Ryu, "Optical design of reflecting omnidirectional zoom optical system with peripheral half-field of view from 110 to 72 for day and night surveillance," *Optik*, vol. 212, Article ID 164690, 2020.

[12] Z. Qin, Y. Qi, and C. Ren, "Desensitization design method for freeform TMA optical systems based on initial structure screening," *Photonics*, vol. 9, no. 8, p. 544, 2022.

[13] X. Bai, G. Ju, and H. Ma, "Aberrational interactions between axial and lateral misalignments in pupil-offset off-axis two-mirror astronomical telescopes," *Applied Optics*, vol. 58, no. 28, pp. 7693–7707, 2019.

[14] X. Zhang, L. Zheng, and X. He, "Design and fabrication of imaging optical systems with freeform surfaces," *Proceedings of SPIE- The International Society for Optical Engineering*, vol. 8486, no. 4, Article ID 848607, 2012.

[15] B. Z. Pan, J. Tang, A. H. Wang, and X. Y. Dong, "Design strategy for flat-field Schmidt optical system," *Optik*, vol. 125, no. 4, pp. 1585–1588, 2014.

[16] Y. Wang, H. Yang, and K. Xie, "Design for high precision and off-axis compact collimation system," *Optik*, vol. 122, no. 2, pp. 122–124, 2011.